Atomic-level characterization of protein–protein association

Albert C. Pan[a,1], Daniel Jacobson[a], Konstantin Yatsenko[a], Duluxan Sritharan[a], Thomas M. Weinreich[a], and David E. Shaw[a,b,1]

[a]D. E. Shaw Research, New York, NY 10036; and [b]Department of Biochemistry and Molecular Biophysics, Columbia University, New York, NY 10032

Despite the biological importance of protein–protein complexes, determining their structures and association mechanisms remains an outstanding challenge. Here, we report the results of atomic-level simulations in which we observed five protein–protein pairs repeatedly associate to, and dissociate from, their experimentally determined native complexes using a molecular dynamics (MD)–based sampling approach that does not make use of any prior structural information about the complexes. To study association mechanisms, we performed additional, conventional MD simulations, in which we observed numerous spontaneous association events. A shared feature of native association for these five structurally and functionally diverse protein systems was that if the proteins made contact far from the native interface, the native state was reached by dissociation and eventual reassociation near the native interface, rather than by extensive interfacial exploration while the proteins remained in contact. At the transition state (the conformational ensemble from which association to the native complex and dissociation are equally likely), the protein–protein interfaces were still highly hydrated, and no more than 20% of native contacts had formed.

molecular dynamics simulations | enhanced sampling | protein–protein association

Most proteins associate with other proteins to function, forming complexes that lie at the heart of nearly all physiological processes, including signal transduction, DNA repair, enzyme inhibition, and the immune response. Determining the structures of these complexes and elucidating their association mechanisms are problems of fundamental importance. While substantial progress has been made toward the structural determination of protein–protein complexes, such structures are still relatively underrepresented in the Protein Data Bank (1), especially compared with the large number of known, functional protein–protein interactions derived from high-throughput, nonstructural approaches like yeast two-hybrid screening and affinity purification–mass spectrometry (2). Moreover, the structures of many complexes that are important drug targets for cancer and autoimmune disease remain difficult to determine experimentally (3, 4). As for protein–protein association mechanisms, powerful experimental approaches like double-mutant cycles and paramagnetic relaxation enhancement have afforded a wealth of information about potential transition states and intermediates (5, 6), but these data are often indirect or limited to, for example, metalloproteins or proteins with attached paramagnetic spin labels. Obtaining direct, atomic-level detail about association pathways for a diverse set of protein–protein complexes and developing broader insights into the common principles of protein–protein association mechanisms are still open problems.

Atomic-level molecular dynamics (MD) simulations offer a computational route toward characterizing both the structure and dynamics of protein–protein complexes. Using MD, one could in principle start a simulation with two protein monomers and "watch" them associate and dissociate reversibly during a single trajectory. Such a simulation would provide an unprecedented sampling of the possible complexes that can be formed by the protein monomers and a straightforward way to rank the stability of different complexes based on that fraction of the time during which each complex is observed. Moreover, mechanistic details like intermediate and transition states along the association pathway could be observed. In practice, however, it has proven difficult to study protein–protein association and dissociation in MD simulations: Reversible association during a single simulation trajectory has not been observed at all. Indeed, only a few examples have been reported (7–15) of simulations that successfully captured spontaneous protein–protein association to an experimentally determined complex, and these examples have been limited to examining one system, or to the association of smaller peptides (7, 11, 14). Recently, Plattner et al. (10) were the first to capture association and dissociation of a protein–protein complex (albeit in separate simulations) as part of a large-scale Markov state model study.

Difficulties encountered in protein–protein association simulations include the formation of nonnative associated states with long lifetimes compared with simulation timescales. Such kinetic traps severely hamper the sampling of other states—including states that may be thermodynamically more favorable, and thus more likely to represent the most populated complex at physiological conditions (16, 17). Even if the most thermodynamically stable complex is sampled, observing spontaneous dissociation could require simulations on the order of seconds to days (18). Some approaches have attempted to overcome this timescale problem by combining data from multiple short simulation

Significance

Most proteins associate with other proteins to function, forming complexes that are central to almost all physiological processes. Determining the structures of these complexes and understanding how they associate are problems of fundamental importance. Using long-timescale molecular dynamics simulations, some performed using a new enhanced sampling method, we observed spontaneous association and dissociation of five protein–protein systems to and from their experimentally determined native complexes. By analyzing the simulations of these five systems, which include members of diverse structural and functional classes, we are able to draw general mechanistic conclusions about protein association.

trajectories (10, 12, 14) and have had success in modeling various aspects of protein–protein association. None of these methods, however, has been applied to a broad set of structurally diverse protein–protein systems, making it difficult to draw general conclusions about protein association. Moreover, such methods require an additional layer of modeling to combine the short trajectories and necessarily rest on assumptions that can bias the results toward atypical pathways or miss important conformational states (19, 20).

In this paper, we have used long-timescale MD simulations in combination with a newly developed enhanced sampling approach, which we call "tempered binding," to simulate the reversible association of five structurally and functionally diverse protein–protein systems, and have also performed conventional MD simulations to capture many spontaneous association events. In the tempered binding simulations, we observed each of the protein–protein pairs repeatedly associate to, and dissociate from, their experimentally determined native complexes. The spontaneous association events observed in subsequent conventional MD simulations allowed us to draw general mechanistic conclusions about the association process of the five proteins we studied: We found that if the proteins made contact far from the native interface, the native state was reached by dissociation and eventual reassociation near the native interface, as opposed to extensive exploration of various protein–protein interfaces while the proteins remained in contact. The protein–protein interfaces were still highly hydrated at the transition state, and no more than 20% of native contacts had formed.

Results

Tempered Binding Simulations of Protein–Protein Association Reversibly Visited the Native Complex. We applied tempered binding to six protein–protein systems and observed reversible association in five out of the six systems (*SI Appendix*, Figs. S1 and S4 and Table S1). For the five reversibly associating systems, the most stable complex in the simulation agrees with the complex determined crystallographically within atomic resolution (Fig. 1). [In the sixth protein–protein system, the protein dimer CLC-ec1 (21), we observed association to the experimentally determined complex, but did not observe dissociation on the timescales of our simulations (*SI Appendix*, Fig. S4).] Some of these simulations also sampled alternative bound states that could have functional relevance, and provided quantitative estimates of the free-energy difference between the native state and these alternative states (Fig. 2 and *SI Appendix*, Figs. S2 and S3). Although for this initial study we have limited ourselves to proteins that do not undergo large conformational changes upon binding (*SI Appendix*, Table S1), we note that such proteins in themselves constitute a large class of important protein–protein complexes (22). (The ribonuclease HI–SSB-Ct system could be considered an exception, since the SSB-Ct peptide folds upon binding to the ribonuclease, but the RMSD difference between the folded and disordered forms of the peptide is only about 2 Å.)

In a tempered binding simulation, the strength of interactions between the protein monomer atoms, and sometimes between the protein monomer and solvent atoms, is scaled at regular time intervals using a simulated Hamiltonian tempering framework (14, 23–25). This scaling allows long-lived states to dissociate more quickly. In practice, tempered binding involves a conventional MD simulation augmented by frequent Monte Carlo moves that update the scaling strength among rungs on a ladder of values. The Monte Carlo updates are detail balanced such that, at each rung of the ladder, a Boltzmann distribution of states corresponding to that rung's value of the scaling factor is properly sampled. In particular, the sampling at the lowest rung of the ladder (rung 0) corresponds to the completely unscaled Hamiltonian and is consistent with the distribution of states sampled in a conventional MD simulation.
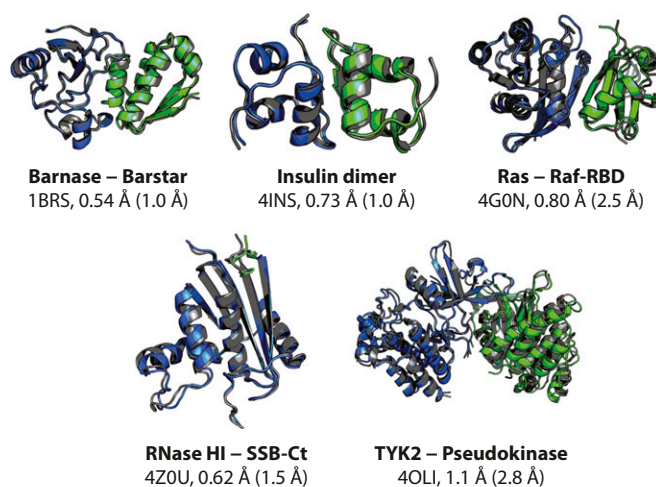
Fig. 1. The most thermodynamically stable complex visited during reversible-association simulations agrees with the experimentally determined complex within atomic resolution. Representative structures of the most thermodynamically stable complexes observed in reversible-association simulations are shown. For each protein–protein complex, we show a representative associated structure obtained from simulation (blue and green) superimposed on the experimentally determined crystal structure (gray) by a best-fit Cα alignment of the larger protein monomer (blue), along with the name of the complex, the Protein Data Bank (PDB) entry of the experimental structure (3, 26, 50–52), and the Cα interface and ligand RMSDs (I-RMSD and L-RMSD) between the two structures. The protein–protein interface is defined as any pair of Cα atoms, one from each protein monomer, within 10 Å of each other in the experimentally determined complex. The I-RMSD is then calculated by aligning the interface Cα atoms of the representative structure and the experimentally determined structure and determining the Cα RMSD of the interface. The L-RMSD is calculated by first aligning the Cα atoms of the larger protein monomer and then calculating the Cα RMSD of the smaller protein monomer (green) (1). Tempered binding simulations for these five protein–protein systems used the Amber ff99SB*-ILDN (37–39) force field and the TIP3P (40) water model. The representative structure was obtained by clustering the simulations, to avoid bias toward the experimentally determined structure. Clustering was only performed on simulation frames sampled at the lowest tempering rung (rung 0), where the distribution of states is the same as that of a conventional MD simulation. The representative structure from the cluster with the greatest occupancy is used in the figure. Because the tempered binding approach scales all interactions uniformly, the simulations were not biased for, or steered toward, any particular protein–protein complex. Although tempered binding successfully recapitulated experimentally determined bound structures for these systems, its computational expense greatly exceeds that of other approaches, such as docking, for this particular task. We note, however, that its accuracy for this set of five complexes is considerably better than a current state-of-the-art docking program, particularly in its ability to select the correct native-like structure among various low-energy protein–protein complexes (*SI Appendix*, Table S3), speaking both to the level of sampling achieved by tempered binding and to the accuracy of current MD force fields. Additional descriptions of the systems and the methods are available in *SI Appendix*.

Our current tempered binding protocol (which focuses on scaling the near electrostatic interactions between protein monomers, between protein monomers and water molecules, and, in the case of CLC-ec1, between protein monomers and lipid molecules) resulted in a significant increase in sampling efficiency in our simulations of the protein–protein systems studied in this work. In a tempered binding simulation of the enzyme–inhibitor system barnase–barstar, for example, the protein–protein system escaped from its native complex in hundreds of microseconds (*SI Appendix*, Fig. S1), whereas the lifetime of the native complex is on the order of a day (26), a speedup of almost nine orders of magnitude. It is possible, however, that other tempered binding protocols might further improve sampling
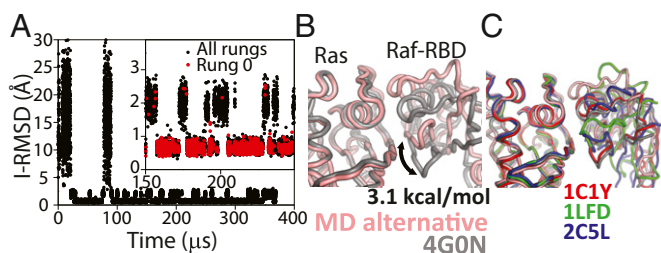
Fig. 2. Tempered binding provides a direct atomic-level observation of the ensemble of bound states involved in protein–protein interactions. (*A*) An I-RMSD trace of a tempered binding simulation of the Ras protein binding to the Ras-binding domain of the Raf effector protein (Raf-RBD) shows reversible association to the crystal complex (PDB ID code 4G0N) (51). For Ras–Raf-RBD, the simulation not only reached the known crystal–structure complex, which was the most thermodynamically stable state, but also an alternative complex about 2 Å away from the crystal structure. The *Inset* shows a portion of the RMSD trace zoomed in along the *y* axis. Black (red) circles are points from all (rung 0) trajectory frames. (*B*) A structure of the alternative state (pink) overlaid onto the crystal structure (gray), aligned to the Ras domain, is shown. Counting the population of the crystal-like state versus the alternative state in rung 0 suggests that the alternative state is ~3.1 kcal·mol^{-1} higher in free energy than the crystal-like state. (*C*) An overlay of other Ras–effector complexes demonstrates that the conformation of this alternative state is well within the range of observed binding-interface conformations (53–55).

efficiency and perhaps allow us to observe reversible association for the CLC-ec1 dimer (*SI Appendix*, Fig. S4).

Conventional MD Simulations Captured Spontaneous Protein–Protein Association to the Native Complex and Revealed a Shared Association Mechanism. In addition to the tempered binding simulations, we performed hundreds of conventional MD simulations of the five reversibly associating protein systems to study their association mechanisms (Table 1). In each of these simulations, we observed the proteins come into contact and form loosely associated protein–protein configurations (encounter complexes) that then either (*i*) formed the specific, close-range interactions in the native complex without the proteins at any point dissociating (a successful association event), (*ii*) dissociated without first reaching the native complex (an unsuccessful association event), or (*iii*) remained kinetically trapped in a nonnative state for the remainder of the simulation. (Here, we use the term "encounter complex" to refer to the set of protein–protein configurations in which any heavy atom in one protein is within 4.5 Å of any heavy atom in the other protein, but in which the interface RMSD is not within 1.5 Å of the native

complex.) In some simulations, there were unsuccessful association events preceding a successful association event. We note that we observed several successful association events for each of the five systems (Table 1), and, as expected, we observed no examples of dissociation once the experimentally determined complex formed.

Successful association events in these five systems shared several key features. Rather than forming an encounter complex at a random interface and reaching the native interface (without dissociating) by way of an extensive search, in successful association events the encounter complexes tended to form near the native interface, at least for events observed within the timescale of our simulations (on the order of tens of microseconds). (For a given protein–protein system, the contact preceding a successful association event tended to be nonspecific, varying among different events, but typically involved interactions between charged residues in or close to the native binding interface.) In contrast, encounter complexes that formed during unsuccessful association events displayed a wide variety of relative protein–protein positions, with no pronounced preference for their positions in the native complex (Fig. 3 and *SI Appendix*, Fig. S5).
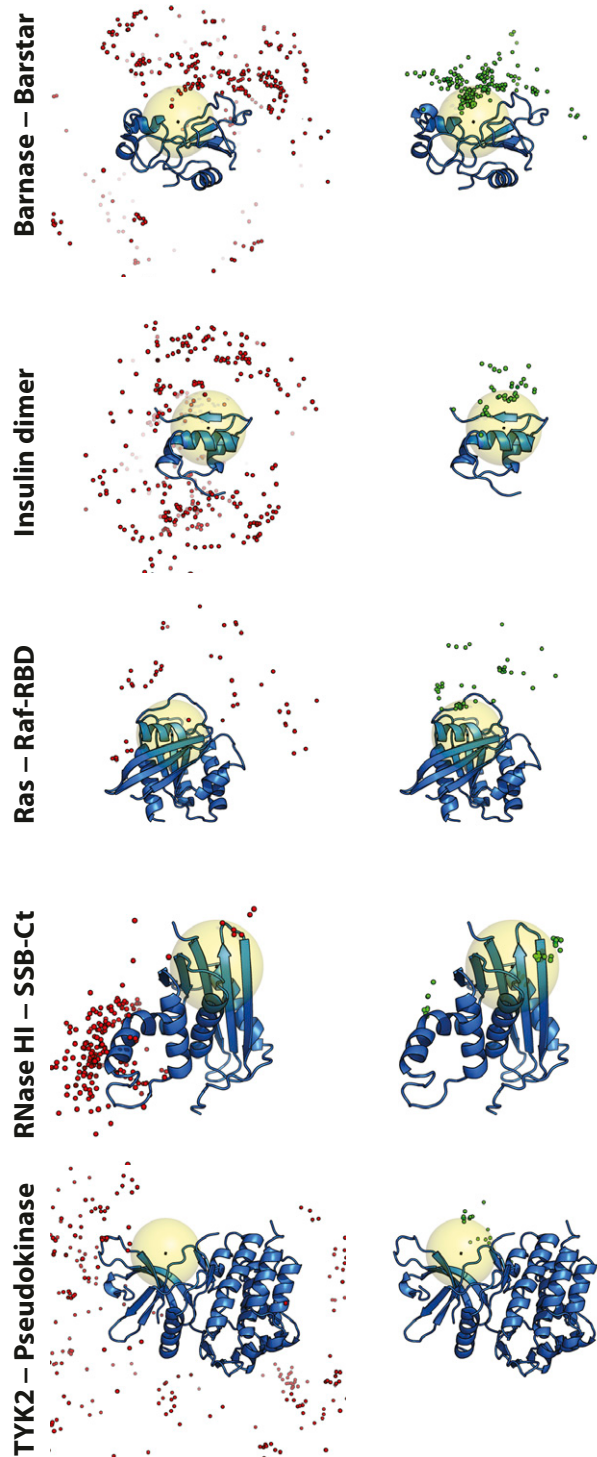
Successful association events in the five systems also shared similar features at the transition state (the ensemble of configurations from which association and dissociation are equally likely): No more than 20% of native contacts had formed in these configurations, and the protein–protein interfaces were still highly hydrated. We identified configurations in the transition state ensemble of association by calculating the probability of successful association, p_{Assoc} (also known as the committor probability), for several configurations during a successful association event (27, 28), and were able to identify configurations at or near the transition state for all five systems. A configuration is classified as a member of the transition state ensemble if $p_{Assoc} = 50\%$ (that is, if additional trajectories initiated from that configuration with randomized velocities drawn from a Boltzmann distribution commit half of the time to the native complex and half of the time to the unbound state). All of the transition states characterized here occurred when <20% of native contacts had formed and while there were still a significant number of water molecules between atoms that are in contact in the native complex (Fig. 4). Given the intensive computational effort required for determining committor probabilities and identifying transition states, we only determined committor values in one successful association event for each system condition. The general features of the transition state configurations were found to be qualitatively similar among simulations of barnase–barstar with different force fields (Table 1), and even among completely different systems (Fig. 4D), however, providing strong evidence that these transition states are representative of the transition state ensembles for these five systems.

Table 1. List of conventional MD simulations of spontaneous protein–protein association

Condition	System	No. of trajectories/successful association events	Aggregate time, μs	Association rate, M^{-1}·s^{-1}
BB_1	Barnase–barstar	61/24	440	2.3(2) × 10^7
BB_2		61/28	212.7	6(1) × 10^7
BB_3		51/3	225	4.4 × 10^6
IND_2	Insulin dimer	61/6	294.8	4.1 × 10^6
RAS_1	Ras–Raf-RBD	81/7	117	2.6 × 10^7
RNA_1	RNase HI–SSB-Ct	51/5	294	1.0 × 10^7
TYK_2	TYK2-Pseudokinase	151/3	461	4.2 × 10^6

Simulations were initiated with different velocities from the same configuration with the two proteins unbound (different association pathways of the two proteins were sampled, providing strong evidence that the choice of starting positions does not influence the binding events; *SI Appendix*, Fig. S6). A successful association event is defined as a trajectory in which the I-RMSD between the two proteins and the experimentally determined complex structure became less than 1.5 Å after the RMSD time series was smoothed with a 10-ns moving average. Over 2 ms of aggregate simulation time was used for these spontaneous association trajectories. The experimental rates of association for barnase–barstar and insulin dimer are 6.0 × 10^8 M^{-1}·s^{-1} (32) and 1.14 × 10^8 M^{-1}·s^{-1} (56), respectively. For Ras–Raf-RBD, at least three different experimental association rate estimates are available: 4.5 × 10^7 M^{-1}·s^{-1} (57), 5.9 × 10^6 M^{-1}·s^{-1} (58), and 1.02 × 10^4 M^{-1}·s^{-1} (59). We were unable to find experimental rates of association for RNase HI–SSB-Ct or TYK2-Pseudokinase.

Unsuccessful association   Successful association

Barnase – Barstar

Insulin dimer

Ras – Raf-RBD

RNase HI – SSB-Ct

TYK2 – Pseudokinase

Fig. 3. Encounter complexes visited in successful association events favored structures in which the two proteins were positioned similarly to how they are positioned in the experimentally determined complex. Simulation frames were uniformly sampled from encounter complexes and aligned to the larger protein. A single snapshot of the larger protein (blue cartoon) is shown for reference, overlaid with multiple snapshots of a Cα atom of the smaller protein near the center of the native binding interface taken from unsuccessful (red spheres) and successful (green spheres) association trajectories. The large yellow sphere indicates a region defined by a 10-Å radius around the center of mass of the binding interface of the

Discussion

For the enzyme–inhibitor complex barnase–barstar, one of the best experimentally characterized protein–protein complexes (26), our simulations are consistent with previous experimental and computational work, including extensive mutational analysis (5, 29) and Brownian dynamics simulations (30, 31). Combining the information from the tempered binding and conventional MD simulations, we estimated the binding free energy, ΔG_b, to be 19.2(2) kcal·mol^{-1} [$K_d = 1.0(2) \times 10^{-14}$ M], the association rate, k_{on}, to be $2.3(2) \times 10^7$ M^{-1}·s^{-1}, and the dissociation rate, k_{off}, to be $2.3(3) \times 10^{-7}$ s^{-1}. These simulation-derived values correspond relatively well with the known experimental values of $\Delta G_b = 19$ kcal·mol^{-1}, $k_{on} = 6 \times 10^8$ M^{-1}·s^{-1}, and $k_{off} = 8 \times 10^{-6}$ s^{-1} (32). (Further discussion of how the simulation values were calculated can be found in *SI Appendix*.)

Notably, our atomic picture of the transition state agrees with mutational and kinetic studies from Schreiber and coworkers (5, 33), which suggest that the transition state occurs before a majority of native interactions are formed, and while the protein–protein interface is still highly solvated. More recent experimental work on the coupled folding and binding of disordered protein domains also suggests that the majority of native contacts form after the transition state (34).

In addition, our observation that associating proteins already had relative positions similar to those in the native complex upon making contact during successful simulated association events is consistent with the idea of a so-called "funneled" association process, in which long-range electrostatic attraction is involved in the rapid association of barnase–barstar (31, 35) and other protein–protein pairs with oppositely charged binding sites (36). This observation is also consistent with previous atomistic MD simulation studies of protein–peptide binding, in which successful association pathways tended to be funnel-like, often due to electrostatic steering (7, 11, 14). Relatedly, in a recent simulation study of a peptide binding to the PDZ domain, multiple binding and unbinding events were observed before successful association, and the peptide did not extensively search the surface while bound (11).

The strong affinity of barstar for barnase and the hydrophilic nature of the interface make it a relatively unusual protein–protein system, so it is striking that the features of the transition state and encounter complex observed in our simulations were common to the association mechanisms of all of the protein–protein systems studied in this work (Fig. 4). This shared mechanism may thus also apply to the broader class of protein–protein complexes that—like the systems studied here (*SI Appendix*, Table S1)—do not undergo large conformational changes upon binding.

We have observed reversible association of a set of five protein–protein systems to their respective experimentally determined structures using an enhanced sampling method that enabled an increase in sampling efficiency of as much as nine orders of magnitude. Together with our long-timescale conventional MD simulations, which yielded many spontaneous association events, our results provide an atomic-level view of protein–protein association mechanisms. In the future, this methodology could be used to determine the structures and association mechanisms of at least some protein–protein complexes that have not yet been experimentally characterized. The ability to observe both association and dissociation events could be especially useful in this context, helping to distinguish thermodynamically stable complexes from kinetically trapped states that are sparsely populated.

larger protein. Kinetically trapped nonnative states, which neither dissociated nor reached the native state during a simulation, were not included in this analysis.

Fig. 4. The transition state for association was solvated, and only <20% of native contacts had formed. Configurations and portions of I-RMSD traces from successful association events in conventional MD simulations of (*A*) barnase–barstar and (*B*) RNase HI–SSB-Ct association are shown. The green arrows indicate points where p_{Assoc} was calculated in the successful association event (red circles). The *Insets* show an expanded view of the region close to the transition state, showing the fraction of native contacts (black) and fractional hydration around the interface (blue) as a function of time (*SI Appendix*). Additional configurations near the transition state of association are shown for (*C*) insulin dimer, Ras–Raf-RBD, and TYK2-pseudokinase. Configurations show the larger protein as a blue cartoon, the smaller protein as a green cartoon, interprotein residue contacts between residues at the native interface as van der Waals spheres, and water within 4 Å of the native binding interfaces as red and white licorice, demonstrating the lack of protein–protein contacts and the large amount of water at the binding interface. (*D*) A plot of the probability of association, p_{Assoc}, against the fraction of native contacts and a normalized water interface coordinate (*Inset*). The fraction of native contacts remained below 30% even for configurations that had a committor probability of 90% to the native-complex state. Protein–protein interfaces in the successful association events, except for insulin dimer, which has a relatively hydrophobic interface, also remained more than 50% solvated. We note that these observations about the fraction of native contacts and interface solvation are qualitatively similar for the transition state of barnase–barstar determined under three different force field conditions: BB_0, BB_2, and BB_3 (*SI Appendix*, Fig. S7).

Methods

MD Simulations. Simulations were based on the crystal structures of the protein complexes listed in *SI Appendix*, Table S1. Unless otherwise indicated, Lys, Arg, Asp, and Glu residues, as well as the N and C termini, were simulated in their charged states, and all His residues were neutral. For the soluble proteins, structures were solvated with water molecules, and counterions were added until the system was overall neutral. We used the Amber ff99SB*-ILDN (37–39) force field and the TIP3P (40) water model for these simulations, except for a few simulations of barnase–barstar, in which we also used the four-site water model TIP4P/2005 (41) as a control. The Ras–Raf-RBD system contained the ligand GppNHp, a GTP analog, and the TYK2-pseudokinase system contained two copies of the ligand compound 7012, a TYK2 inhibitor. These ligands were parameterized with the generalized Amber force field (42).

For the membrane–protein dimer system CLC-ec1, we truncated the dynamic N-terminal helix (residues 17–30) on both monomers, and inserted the system into a palmitoyl oleoyl phosphatidylethanolamine (POPE) lipid bilayer. The CHARMM27 force field was used for the protein, ions, and water (43, 44), and the CHARMM36 force field for lipids (45). We also adjusted the side-chain charges of aspartate, glutamate, and arginine residues ("DER" correction) to weaken the guanidinium acetate association constant (46).

For some of our protein–protein systems, we applied torsional corrections to the φ and ψ backbone dihedrals, consisting of an additional potential $U = k \sum_{m=1}^{M} (-1)^{m-1}[(1 + \cos m(\varphi - \varphi'))/m!]$ ($M = 6$), where k ranged from 1 to 5 kcal·mol^{-1}, and the cosine terms were centered at $\varphi' = \varphi_{xtal} - 180°$. This term adds a backbone restraint and helps prevent system degradation on the microsecond timescale (46). Even with the addition of these terms, the protein backbone is able to fluctuate, and, more importantly, protein side chains retain full flexibility. We observed, for example, subtle but significant side-chain fluctuations at the barnase–barstar binding interface (*SI Appendix*, Fig. S2). Specific values of k, the backbone dihedrals to which this correction was applied, further justification for these terms, and additional simulation details can be found in *SI Appendix*.

Tempered Binding. To enhance the sampling in our protein–protein association simulations, we used an approach that we call tempered binding, which is analogous to simulated tempering (47, 48), except that terms in the system's energy function, as opposed to its temperature, are updated during the simulation. Tempered binding dynamically scales various atomic interactions during an MD simulation by a factor, λ, that is updated among a ladder of discrete values, λ_i. At the lowest rung of the ladder (rung 0), the atomic interactions are unscaled (i.e., $\lambda_0 = 1$). An update attempt was

performed in two steps. First, the following normalized probability distribution was calculated for the given atomic configuration, x:

$$p(\lambda_i) = \frac{\exp(-\beta H_i(x) + f_i)}{\sum_j \exp(-\beta H_j(x) + f_j)}.$$

Here, $\beta = (k_B T)^{-1}$, k_B is Boltzmann's constant, T is temperature, H_i is the energy function, or Hamiltonian, at rung λ_i, and f_i is a free-energy weight at rung i, calculated adaptively during the simulation. Second, a new rung was chosen with a probability consistent with $p(\lambda_i)$ (49). Our tempered binding simulations scaled near electrostatic and van der Waals nonbonded interactions between different groups of atoms in the system. Additional details about tempered binding can be found in *SI Appendix*.

1. Lensink MF, et al. (2016) Prediction of homoprotein and heteroprotein complexes by protein docking and template-based modeling: A CASP-CAPRI experiment. *Proteins* 84:323–348.
2. Vidal M, Cusick ME, Barabási A-L (2011) Interactome networks and human disease. *Cell* 144:986–998.
3. Lupardus PJ, et al. (2014) Structure of the pseudokinase-kinase domains from protein kinase TYK2 reveals a mechanism for Janus kinase (JAK) autoinhibition. *Proc Natl Acad Sci USA* 111:8025–8030.
4. Shan Y, et al. (2014) Molecular basis for pseudokinase-dependent autoinhibition of JAK2 tyrosine kinase. *Nat Struct Mol Biol* 21:579–584.
5. Frisch C, Fersht AR, Schreiber G (2001) Experimental assignment of the structure of the transition state for the association of barnase and barstar. *J Mol Biol* 308:69–77.
6. Tang C, Iwahara J, Clore GM (2006) Visualization of transient encounter complexes in protein-protein association. *Nature* 444:383–386.
7. Ahmad M, Gu W, Helms V (2008) Mechanism of fast peptide recognition by SH3 domains. *Angew Chem Int Ed Engl* 47:7626–7630.
8. Ahmad M, Gu W, Geyer T, Helms V (2011) Adhesive water networks facilitate binding of protein interfaces. *Nat Commun* 2:261.
9. Schmidt AG, et al. (2013) Preconfiguration of the antigen-binding site during affinity maturation of a broadly neutralizing influenza virus antibody. *Proc Natl Acad Sci USA* 110:264–269.
10. Plattner N, Doerr S, De Fabritiis G, Noé F (2017) Complete protein-protein association kinetics in atomic detail revealed by molecular dynamics simulations and Markov modelling. *Nat Chem* 9:1005–1011.
11. Blöchliger N, Xu M, Caflisch A (2015) Peptide binding to a PDZ domain by electrostatic steering via nonnative salt bridges. *Biophys J* 108:2362–2370.
12. Saglam AS, Wang DW, Zwier MC, Chong LT (2017) Flexibility vs preorganization: Direct comparison of binding kinetics for a disordered peptide and its exact preorganized analogues. *J Phys Chem B* 121:10046–10054.
13. Piana S, Lindorff-Larsen K, Shaw DE (2013) Atomistic description of the folding of a dimeric protein. *J Phys Chem B* 117:12935–12942.
14. Paul F, et al. (2017) Protein-peptide association kinetics beyond the seconds timescale from atomistic simulations. *Nat Commun* 8:1095.
15. Liu P, Huang X, Zhou R, Berne BJ (2005) Observation of a dewetting transition in the collapse of the melittin tetramer. *Nature* 437:159–162.
16. Gumbart JC, Roux B, Chipot C (2013) Efficient determination of protein-protein standard binding free energies from first principles. *J Chem Theory Comput* 9:3789–3798.
17. Abriata LA, Dal Peraro M (2015) Assessing the potential of atomistic molecular dynamics simulations to probe reversible protein-protein recognition and binding. *Sci Rep* 5:10549.
18. Vreven T, et al. (2015) Updates to the integrated protein-protein interaction benchmarks: Docking benchmark version 5 and affinity benchmark version 2. *J Mol Biol* 427:3031–3041.
19. Fersht AR (2002) On the simulation of protein folding by short time scale molecular dynamics and distributed computing. *Proc Natl Acad Sci USA* 99:14122–14125.
20. Paci E, Cavalli A, Vendruscolo M, Caflisch A (2003) Analysis of the distributed computing approach applied to the folding of a small β peptide. *Proc Natl Acad Sci USA* 100:8217–8222.
21. Dutzler R, Campbell EB, Cadene M, Chait BT, MacKinnon R (2002) X-ray structure of a ClC chloride channel at 3.0 Å reveals the molecular basis of anion selectivity. *Nature* 415:287–294.
22. Zhou HX, Bates PA (2013) Modeling protein association mechanisms and kinetics. *Curr Opin Struct Biol* 23:887–893.
23. Sugita Y, Kitao A, Okamoto Y (2000) Multidimensional replica-exchange method for free-energy calculations. *J Chem Phys* 113:6042–6051.
24. Fukunishi H, Watanabe O, Takada S (2002) On the Hamiltonian replica exchange method for efficient sampling of biomolecular systems. *J Chem Phys* 116:9058–9067.
25. Liu P, Kim B, Friesner RA, Berne BJ (2005) Replica exchange with solute tempering: A method for sampling biological systems in explicit water. *Proc Natl Acad Sci USA* 102:13749–13754.
26. Buckle AM, Schreiber G, Fersht AR (1994) Protein-protein recognition: Crystal structural analysis of a barnase-barstar complex at 2.0-Å resolution. *Biochemistry* 33:8878–8889.
27. Bolhuis PG, Chandler D, Dellago C, Geissler PL (2002) Transition path sampling: Throwing ropes over rough mountain passes, in the dark. *Annu Rev Phys Chem* 53:291–318.
28. Du R, et al. (1998) On the transition coordinate for protein folding. *J Chem Phys* 108:334–350.
29. Schreiber G, Fersht AR (1995) Energetics of protein-protein interactions: Analysis of the barnase-barstar interface by single mutations and double mutant cycles. *J Mol Biol* 248:478–486.
30. Spaar A, Dammer C, Gabdoulline RR, Wade RC, Helms V (2006) Diffusional encounter of barnase and barstar. *Biophys J* 90:1913–1924.
31. Gabdoulline RR, Wade RC (2002) Biomolecular diffusional association. *Curr Opin Struct Biol* 12:204–213.
32. Schreiber G, Fersht AR (1993) Interaction of barnase with its polypeptide inhibitor barstar studied by protein engineering. *Biochemistry* 32:5145–5150.
33. Schreiber G (2002) Kinetic studies of protein-protein interactions. *Curr Opin Struct Biol* 12:41–47.
34. Dogan J, Mu X, Engström Å, Jemth P (2013) The transition state structure for coupled binding and folding of disordered protein domains. *Sci Rep* 3:2076.
35. Schreiber G, Fersht AR (1996) Rapid, electrostatically assisted association of proteins. *Nat Struct Biol* 3:427–431.
36. Long D, Brüschweiler R (2013) Directional selection precedes conformational selection in ubiquitin-UIM binding. *Angew Chem Int Ed Engl* 52:3709–3711.
37. Hornak V, et al. (2006) Comparison of multiple amber force fields and development of improved protein backbone parameters. *Proteins* 65:712–725.
38. Best RB, Hummer G (2009) Optimized molecular dynamics force fields applied to the helix-coil transition of polypeptides. *J Phys Chem B* 113:9004–9015.
39. Lindorff-Larsen K, et al. (2010) Improved side-chain torsion potentials for the amber ff99SB protein force field. *Proteins* 78:1950–1958.
40. Jorgensen WL, et al. (1983) Comparison of simple potential functions for simulating liquid water. *J Chem Phys* 79:926–935.
41. Abascal JL, Vega C (2005) A general purpose model for the condensed phases of water: TIP4P/2005. *J Chem Phys* 123:234505.
42. Wang J, Wolf RM, Caldwell JW, Kollman PA, Case DA (2004) Development and testing of a general amber force field. *J Comput Chem* 25:1157–1174.
43. MacKerell AD, Jr, et al. (1998) All-atom empirical potential for molecular modeling and dynamics studies of proteins. *J Phys Chem B* 102:3586–3616.
44. Mackerell AD, Jr, Feig M, Brooks CL, 3rd (2004) Extending the treatment of backbone energetics in protein force fields: Limitations of gas-phase quantum mechanics in reproducing protein conformational distributions in molecular dynamics simulations. *J Comput Chem* 25:1400–1415.
45. Klauda JB, et al. (2010) Update of the CHARMM all-atom additive force field for lipids: Validation on six lipid types. *J Phys Chem B* 114:7830–7843.
46. Jensen MØ, et al. (2012) Mechanism of voltage gating in potassium channels. *Science* 336:229–233.
47. Marinari E, Parisi G (1992) Simulated tempering: A new Monte Carlo scheme. *Europhys Lett* 19:451–458.
48. Lyubartsev AP, Martsinovski AA, Shevkunov SV, Vorontsov-Velyaminov PN (1992) New approach to Monte Carlo calculation of the free energy: Method of expanded ensembles. *J Chem Phys* 96:1776–1783.
49. Chodera JD, Shirts MR (2011) Replica exchange and expanded ensemble simulations as Gibbs sampling: Simple improvements for enhanced mixing. *J Chem Phys* 135:194110.
50. Petzold C, Marceau AH, Miller KH, Marquee S, Keck JL (2015) Interaction with single-stranded DNA-binding protein stimulates *Escherichia coli* ribonuclease HI enzymatic activity. *J Biol Chem* 290:14626–14636.
51. Fetics SK, et al. (2015) Allosteric effects of the oncogenic RasQ61L mutant on Raf-RBD. *Structure* 23:505–516.
52. Baker EN, et al. (1988) The structure of 2Zn pig insulin crystals at 1.5 Å resolution. *Philos Trans R Soc Lond B Biol Sci* 319:369–456.
53. Nassar N, et al. (1995) The 2.2 Å crystal structure of the Ras-binding domain of the serine/threonine kinase c-Raf1 in complex with Rap1A and a GTP analogue. *Nature* 375:554–560.
54. Huang L, Hofer F, Martin GS, Kim SH (1998) Structural basis for the interaction of Ras with RalGDS. *Nat Struct Biol* 5:422–426.
55. Bunney TD, et al. (2006) Structural and mechanistic insights into ras association domains of phospholipase C epsilon. *Mol Cell* 21:495–507.
56. Koren R, Hammes GG (1976) A kinetic study of protein-protein interactions. *Biochemistry* 15:1165–1171.
57. Sydor JR, Engelhard M, Wittinghofer A, Goody RS, Herrmann C (1998) Transient kinetic studies on the interaction of Ras and the Ras-binding domain of c-Raf-1 reveal rapid equilibration of the complex. *Biochemistry* 37:14292–14299.
58. Yoo J, Lee TS, Choi B, Shon MJ, Yoon TY (2016) Observing extremely weak protein-protein interactions with conventional single-molecule fluorescence microscopy. *J Am Chem Soc* 138:14238–14241.
59. Fischer A, et al. (2007) B- and C-RAF display essential differences in their binding to Ras: The isotype-specific N terminus of B-RAF facilitates Ras binding. *J Biol Chem* 282:26503–26516.

BIOPHYSICS AND COMPUTATIONAL BIOLOGY